ARCHIVES OF ELECTRICAL ENGINEERING VOL. 75(1), pp. 157–175 (2026)

DOI 10.24425/aee.2026.156807

A novel maximum power point tracking approach for stand-alone PV/Wind-Battery Hybrid System

SALHI FATIMA, HAMIDIA FETHIA, ABBADI AMEL, TLEMCANI ABDELHALIM ✉

Faculty of Technology, Electrical Engineering Department
Yahia Feres, Medea University
Ouzera Pole, Medea, Algeria

e-mail: {hamidia.fethia/abbadi.amel/salhi.fatima/✉ tlemcani.abdelhalim}@univ-medea.dz

(Received: 30.08.2025, revised: 27.01.2026)

Abstract: This study explores the implementation of a novel Maximum Power Point Tracking (MPPT) algorithm, referred to as the Tribal Intelligent Evolutionary Optimization (TIEO) algorithm, for concurrent MPPT in both photovoltaic (PV) systems, subject to irradiance and temperature variations, and wind energy systems, affected by variation in wind speed. The principal objective is to maximize the energy extraction from each renewable source under dynamically changing environmental conditions, thereby enhancing overall system performance and energy efficiency. The TIEO algorithm was subsequently implemented and simulated within the MATLAB/Simulink environment for a stand-alone hybrid PV/Wind system incorporating a storage battery. Analysis of the simulation results indicates that the TIEO-based MPPT strategy exhibits high effectiveness, strong adaptability to variable operating conditions, and superior tracking accuracy. Consequently, it presents a promising and robust solution for the control and energy management of hybrid renewable energy systems.

Key words: battery, hybrid system, MPPT-algorithm, PV panel, TIEO, wind turbine

1. Introduction

The rising global energy demand and the diminishing reserves of carbon-based fuels have driven significant research into the development and integration of sustainable and renewable energy technologies. Among the diverse renewable resources, solar and wind energy have garnered particular attention due to their abundance, long-term sustainability, and minimal environmental impact. Photovoltaic (PV) systems are widely accessible, environmentally friendly, require little maintenance, and have continually dropping balance-of-system costs, they have become a top contender for the production of clean energy. The expansion of solar installations has been greatly

aided by ongoing technological advancements and the falling cost of PV modules, especially in small-scale residential applications and low-voltage (LV) distribution networks. In a similar vein, wind energy has become a very competitive and profitable clean energy option. The majority of Wind Energy Conversion Systems (WECSs) in use today use wind turbines with variable speeds, including systems employing an AC generator as a Permanent Magnet Synchronous Generator (PMSG) and a Doubly-fed Induction Generator (DFIG) [1–5]. These configurations are increasingly being adopted in hybrid renewable systems to improve energy reliability and system resilience under constantly changing environmental conditions. Nevertheless, both photovoltaic and wind systems are inherently limited by the stochastic nature of their respective primary energy sources. This inherent intermittency poses major challenges for their operational stability, efficiency, and integration within existing electrical infrastructures. Therefore, to ensure optimal energy harvesting, various techniques have been developed to enable renewable energy systems to operate at their Maximum Power Points (MPPs). MPPT algorithms can generally be classified into two main categories: conventional and intelligent approaches. Conventional techniques are relatively simple and cost-effective; however, they often suffer from limitations such as low tracking efficiency, slow convergence speed, and significant oscillations around the MPP. To overcome these drawbacks, recent research has increasingly focused on intelligent algorithms, including various metaheuristic optimization methods. These AI approaches provide more adaptive, robust, and efficient MPPT performance. For instance, ANNs are capable of modeling the complex, nonlinear relationships between system inputs and outputs, enabling accurate prediction and tracking of the MPP. In contrast, a fuzzy logic controller FLC is particularly advantageous in scenarios where deriving an exact mathematical model is challenging, and it has gained broad acceptance in microcontroller-based MPPT systems, enhancing tracking precision as well as dynamic responsiveness. Numerous studies have been presented over the years to accomplish optimal power extraction in solar photovoltaic (PV) setups, ranging from traditional approaches (e.g., the perturb-and-observe method) to smart control strategies such as fuzzy logic-based regulation and neural network models, and, more recently, to advanced metaheuristic optimization techniques. Building on this foundation, the present study introduces a new metaheuristic method, called the Tribal Intelligent Evolutionary Optimization (TIEO) algorithm, inspired by the sociocultural dynamics of tribal evolution.

The authors in [6–27] have contributed significantly to the literature on MPPT techniques. Some of these works provide comparative analyses of conventional MPPT methods, highlighting their key differences, while others offer comprehensive reviews of the various MPPT approaches proposed in the field.

A similar trend is observed for MPPT in wind turbine systems, where numerous studies have appeared in academic research addressing various methods for Maximum Power Point Tracking (MPPT) in wind energy conversion. Moreover, a growing body of research has focused on hybrid wind/PV energy systems, which integrate both technologies to improve energy reliability and system efficiency. Over the two past years (2023–2025), most recent studies have focused on developing an advanced Maximum Power Point Tracking (MPPT) technique, predominantly focused on photovoltaic (PV) systems in various configurations, including grid-connected and stand-alone, with limited consideration of hybrid PV–wind–battery integration [28]. For instance, [29] introduced a Deep Q-Network (DQN)-based Global Maximum Power Point Tracking (GMPPT) for PV systems and conducted real-time experiments on a PV array supplying a DC load. Similarly, Yılmaz and Çorapsız [30] developed a smart MPPT controller designed for PV installations operating under

partial shading conditions. Their approach combines optimizable Gaussian Process Regression (GPR) with High-Order Sliding Mode Control (HOSMC), constituting a novel hybrid control strategy. In addition, Koshkarbay *et al*. [31] focused on improving the performance of the Social Spider Optimization (SSO) algorithm to enhance MPPT accuracy and convergence in PV systems. In contrast, several investigations into energy management of grid-connected hybrid PV/wind/battery microgrids [32] have incorporated MPPT mechanisms; however, these are primarily based on conventional artificial intelligence (AI) methods such as neural networks (NNs). Furthermore, the study presented in [33] aims to model and simulate a hybrid PV–wind system using MATLAB/Simulink to evaluate its performance and efficiency under varying environmental conditions, where the reported Total Harmonic Distortion (THD) is 3.5%. Overall, the development of advanced MPPT algorithms remains largely confined to PV-only systems. In this study, the proposed TIEO-MPPT algorithm is investigated as an MPPT strategy for hybrid PV–wind/Battery configurations.

2. Power system model

The proposed work presents a Hybrid Energy System (HES) configuration tailored and designed for standalone applications serving remote and off-grid communities, as shown in Fig. 1. The system combines two renewable energy sources, a photovoltaic (PV) generator and a wind energy (WE) system driven by a Permanent Magnet Synchronous Generator (PMSG), which together act as the primary suppliers for the alternating current (AC) electrical load. To guarantee continuous and dependable power delivery, especially during periods of low solar irradiance and reduced wind availability, the design incorporates a Nickel–metal Hydride (Ni-MH) battery Energy Storage System (ESS) is incorporated. This storage unit functions as a supplementary resource to mitigate energy deficits and maintain supply-demand balance. The architecture also includes several power electronic interfaces, such as a unidirectional DC/DC converter for PV, a dual-directional DC/DC power converter for battery integration, also a three-phase DC/AC converter for load interfacing.

Solar energy is typically harvested during daylight hours, whereas wind energy may be available throughout the day and night, with higher intensities often observed during nocturnal periods depending on local climatic conditions. This temporal complementarity between solar and wind resources enhances the stability and availability of renewable generation. However, the inherently variable and intermittent nature of both energy sources, driven by fluctuating meteorological factors such as irradiance and wind speed, poses a significant challenge for consistent power generation. By combining these two sources within a coordinated HES framework, the system achieves improved energy reliability and sustainability while also enabling a reduction in the required battery storage capacity. The primary goal of the proposed paper is to enhance the overall energy efficiency and dynamic performance of the hybrid system through three strategic innovations. First, a TIEO-MPPT diagram is presented, employing two metaheuristic-based algorithms founded on the Tribal Intelligent Evolutionary Optimization (TIEO) technique to maximize energy harvesting from both the photovoltaic and wind systems. Then, advanced control of power flow is realized through a sophisticated battery regulation approach to ensure optimal energy distribution. Third, the integration of appropriate power electronic converters guarantees efficient and reliable energy delivery to the load under various operating conditions.

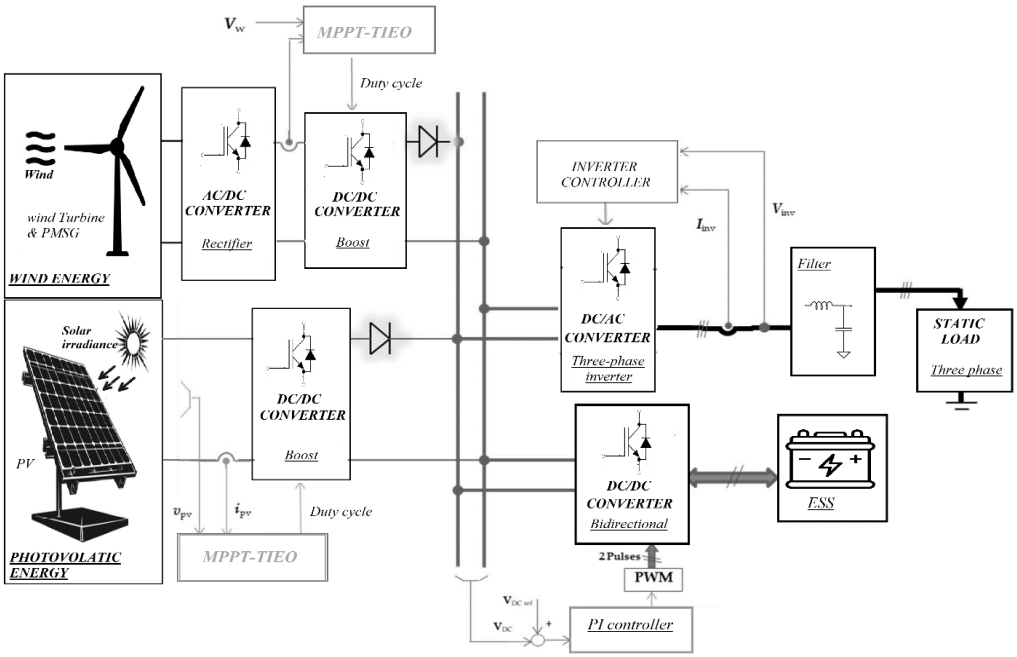

Fig. 1. Schematic of the Standalone Hybrid Power System with TIEO-based MPPT

3. Model description of the PV/wind module

3.1. Photovoltaic system

The ideal case is presented via a parallel connection of a current source and a diode; the real case of a PV cell is represented by the insertion of the resistances R_{se} and R_{pa} as shown in Eq. (1)

$$I = I_{ph} - I_o \left[e^{\left(\frac{V+I*R_{se}}{a*V_{th}}\right)} - 1 \right] - \frac{V + I * R_{pa}}{R_{pa}}. \tag{1}$$

V_{th} is the thermal voltage, V is the PV cell output voltage (V), R_{se} is the cell series resistance (Ω), R_{pa} is the cell parallel resistance (Ω), a is the diode quality factor and I_0 is the diode saturation current (A).

Current-voltage and power-voltage characteristics of the photovoltaic module are illustrated in Fig. 2(b) with temperature and irradiance variation configured with 9 series-connected panels and 9 parallel strings, as implemented in our Hybrid Energy System (HES). It also depicts the synoptic diagram of the PV subsystem, where the photovoltaic generator is interfaced with a dc–dc converter (boost) regulated by a proposed MPPT algorithm. In this configuration, PV-MPPT controller receives the current of photovoltaic (I_{pv}), voltage (V_{pv}) as input variables, and generates the optimized duty cycle (D_{pv}) as its output to regulate power extraction, which is applied to the boost converter via a PWM modulator.

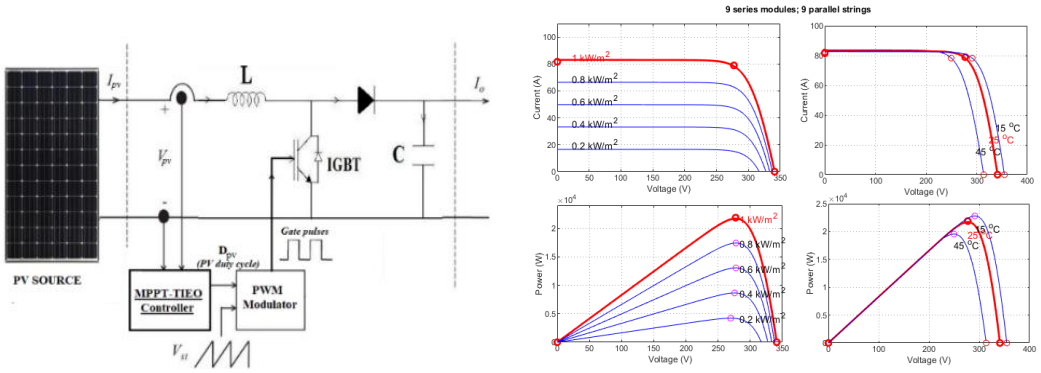

(a) (b)

Fig. 2. (a) Synoptic diagram of the PV source integrated with a boost converter; (b) photovoltaic module characteristic (I-V and P-V curves)

3.2. Wind power generation model

Figure 3 shows the wind turbine's power characteristic curve at a fixed pitch angle ($\beta = 0°$), showing how wind speed and turbine output power are related. Wind energy conversion system's schematic diagram, which shows a wind turbine mechanically connected to a Permanent Magnet Synchronous Generator (PMSG), is also included in the figure. A diode bridge rectifier is used to correct the produced three-phase AC power before it is supplied to a DC-DC boost converter. This converter is regulated by an MPPT algorithm based on the Tribal Intelligent Evolutionary Optimization (TIEO) technique. It receives the generator-side current and voltage as inputs and produces the optimal duty cycle (D_w), which is applied to the boost converter via a PWM modulator to ensure maximum energy harvesting from the wind power. The following (as shown in Eq. (2)) is an expression for the mechanical power that the turbine extracts [34].

$$P_{\text{turbine}} = \frac{1}{2} C_p\left(\lambda, \beta_p\right) \rho A V_{\text{wind}}^3. \tag{2}$$

P_{turbine}, ρ, C_p, A, r, and V_{wind} are, respectively, the wind speed, air density, power coefficient, swept area ($A = \pi r^2$), turbine output power and turbine blade radius. The tip-speed ratio and pitch angle (β_p), (λ) determine the power coefficient which is written as in Eq. (3)

$$C_p\left(\lambda, \beta_p\right) = c_1\left(\frac{c_2}{\lambda_i} - c_3\beta_p - c_4\right) e^{-\frac{c_5}{\lambda_i}} + c_6\lambda. \tag{3}$$

In the d-q reference frame, these PMSG formulas are expressed as in Eq. (4).

$$\begin{aligned} \frac{\mathrm{d}i_{sd}}{\mathrm{d}t} &= -\frac{R_{ss}}{L_{sd}} i_{sd} + \omega_e \frac{L_{sq}}{L_{sd}} i_{sq} + \frac{1}{L_{sd}} V_{sd}, \\ \frac{\mathrm{d}i_{sq}}{\mathrm{d}t} &= -\frac{R_{ss}}{L_{sq}} i_{sq} + \omega_e \left(\frac{L_{sd}}{L_{sq}} i_{sd} + \frac{1}{L_{sq}} \psi_p\right) + \frac{1}{L_{sq}} V_{sq}. \end{aligned} \tag{4}$$

The rotor's electromagnetic torque can be displayed as in Eq. (5).

$$T_e = \frac{3P}{2}[\psi_p i_{sq} + i_{sq} i_{sd} \left(L_{sd} - L_{sq}\right)]. \tag{5}$$

Here, the currents and voltages of the stator in the d-axis and q-axis are denoted as i_{sd}, i_{sq}, V_{sd}, and V_{sq}, respectively. The fundamental electrical angular frequency of the generator is indicated by the value ω_e. L_d and L_q indicate the stator inductance. P stands for the number of poles, R_{ss} for the stator resistance, and ψ_p for the permanent magnet flux linkage.

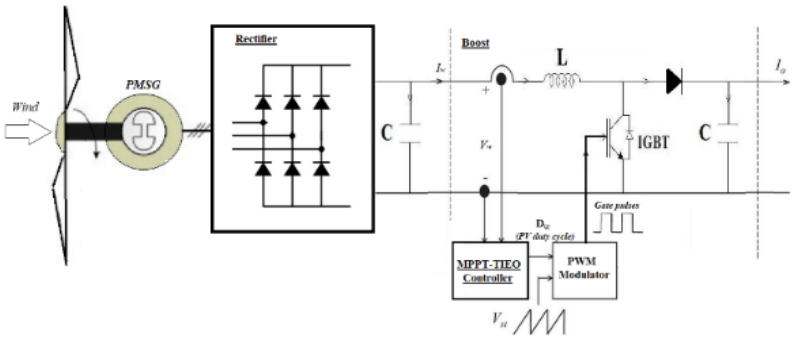

(a)

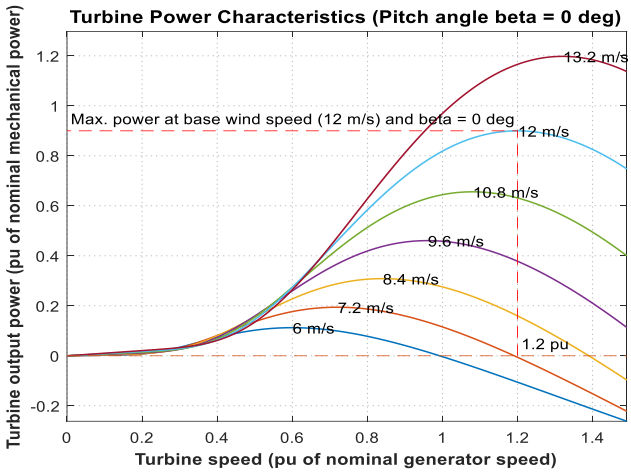

(b)

Fig. 3. (a) Synoptic diagram circuit of the WE conversion system; (b) turbine power characteristics

4. Proposed MPPT-TIEO algorithm

In our study, two independent boost converters are typically employed, one for the photovoltaic (PV) array and the other for the wind energy subsystem. Each source is equipped with a dedicated MPPT controller that calculates the ideal duty ratio to regulate the switching of its respective boost chopper, thereby ensuring efficient power transfer. In the present, we propose TIEO metaheuristic approach introduced by Ye Yao *et al*. in 2025 [35].

The algorithm is inspired by the historical dynamics of tribes dividing and reuniting over time. Within the algorithm, individuals are grouped into tribes using a clustering approach on the basis of the correspondence of their candidate solutions. The best-performing individual in each tribe is appointed as the tribal leader. In each iteration, tribes adopt one of three strategic decision-making modes, autonomy, diplomacy, or war guided by a Q-learning mechanism [36]. This reinforcement learning component enables adaptive learning and intelligent decision-making based on accumulated historical experiences. The operational principle of the proposed metaheuristic approach is presented below and is further illustrated in Fig. 4.

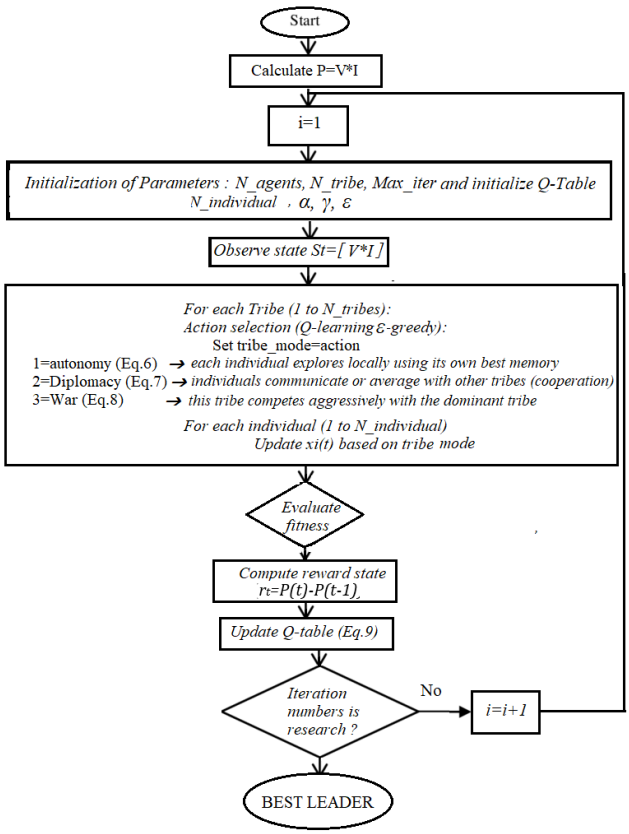

Fig. 4. Flowchart of the proposed TIEO-MPPT algorithm

4.1. Perform autonomy operation

Autonomy denotes the self-driven evolution of governance strategies among individuals within a tribe, guided by their leader's influence. In this mode, each tribe independently explores its own local solution space as shown in Eq. (6).

$$x_i^{(t+1)} = x_i^{(t)} + \alpha * \text{rand}\,() * (x_{\text{tribe}} - x_i^{(t)}), \tag{6}$$

where: $x_i(t)$ is the position of individual i at t, x_{tribe} is the current leader of the tribe, and α is the autonomy learning rate (exploration).

4.2. Perform diplomacy operation

Diplomacy involves the sharing of decision-making strategies between two groups (tribes), in which the leadership approach from one group influences the individuals of the other to varying degrees. This interaction enables tribes to communicate and learn from each other without engaging in conflict as shown in Eq. (7).

$$x_i^{(t+1)} = x_i^{(t)} + \beta * \text{rand}\,() * (x_{\text{other}} - x_i^{(t)}). \tag{7}$$

The different tribe leader with better fitness is presenting by x_{other}, β is the diplomacy factor (moderate learning from others) and rand () is the random value.

4.3. Perform war operation

War refers to the competitive confrontation between tribes, where a stronger tribe can plunder resources from a weaker one. As the conflict escalates, the population of the weaker tribe diminishes, and if it drops to zero, the tribe is eliminated. This process reflects a tribe's attempt to dominate or replace another through competitive pressure as shown in Eq. (8).

$$x_i^{(t+1)} = x_i^{(t)} + \gamma * \text{rand}\,() * (x_{\text{win}} - x_{\text{lose}}), \tag{8}$$

where: x_{win} is the best global leader, x_{lose} is the worst-performing individual in the competing tribe, γ is the war intensity factor (high exploitation) and rand () is the random value.

4.4. Update Q-learning table

Each tribe maintains a Q-table ($Q_i(s,a)$) to learn which strategy works best in each state as shown in Eq. (9).

$$Q\,(s,a) \leftarrow Q\,(s,a) + \eta[r + \zeta \underbrace{\max}_{\acute{a}} Q\,(\acute{s},\acute{a}) - Q\,(s,a)]. \tag{9}$$

The agent observes the current state $s_t = [V_{pv}, I_{pv}]$ in the case of the PV system and $s_t = [V_w, I_w]$ in the case of the wind system, based on this state, the agent selects an action a_t (that mean a perturbation to the duty cycle D_{pv} or D_w). r is the reward $r(t) = P(t) - P(t-1)$, η is the learning rate, and ς is the discount factor. To select an action, we use ε-greedy policy, this strategy maintains a balance between exploring new actions and exploiting the most promising known actions.

Meaning of the Epsilon-Greedy Action Selection

– Explore: the agent ignores the Q-table (it chooses a random action, avoid getting stuck)
– Exploit: the agent chooses the action with the highest Q-value for current state (pick the best action according to what it has leaned so far)

5. Energy Storage System (ESS) model

As shown in Fig. 1, the system architecture integrates multiple coordinated controllers, including the hybrid MPPT controllers, the DC-link voltage controller, and the load-side inverter controller, and is supported by the Energy Storage System (ESS), which plays a critical role in maintaining system stability and ensuring reliable operation under varying generation and load conditions. The DC link voltage is intended to be regulated at 640 V using the suggested battery control approach, starting from an initial battery charge level of 60% State of Charge (SOC). The control combines PI-based voltage regulation, hysteresis current tracking, and SOC supervision. Specifically, the error signal obtained by comparing the reference voltage (V_{dc} = 640 V) and the actual DC voltage is processed by a PI controller to generate a dynamic reference for battery current (I^*_{bat}). A hysteresis comparator then compares this reference with the actual battery current (I_{bat}) to determine whether charging should occur, enabling charging (S_1 = 1) only when the current is below the desired value by a safe margin. Discharging is permitted (S_2 = 1) only when charging is inactive and the SOC remains below a specified upper limit (e.g., 80%), to prevent over-discharge and maintain battery integrity (Fig. 5(b)).

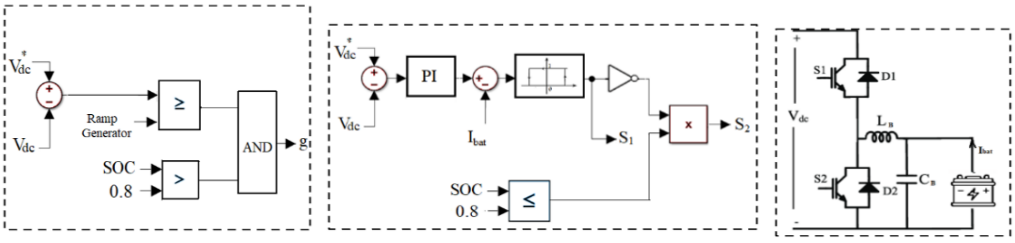

(a) (b) (c)

Fig. 5. (a) The schematic diagram of dump load controller; (b) SE-DC-link voltage controller via (c) DC-DC bidirectional converter

Following this, control signals S_1 and S_2 are then used to regulate the switches of the bidirectional dc–dc converter (Fig. 5(c)), allowing power to flow in or out of the battery accordingly. This intelligent coordination ensures stable power flow in the system (Fig. 6), protects the battery, and keep the DC voltage near to its rated value.

In parallel with battery control, a dump load controller is implemented to safely absorb excess energy when renewable generation surpasses the load requirement and the battery is unable to store additional power (Fig. 5(a)).

On the load side, the Phase-Locked Loop is a widely used DC–AC controller that generates internal sine and cosine references to establish a stable rotating reference frame

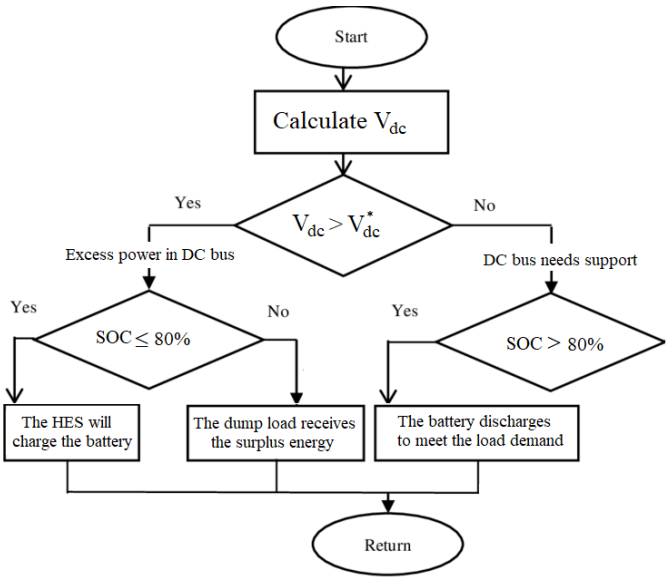

Fig. 6. Flowchart of energy management based on battery bank's SOC limits

6. Results and discussion

To validate the effectiveness of the proposed system, it is first tested on a configuration composed of five photovoltaic (PV) panels connected to a resistive DC load under strong partial shading conditions. Since the proposed technique combines a metaheuristic optimization strategy with reinforcement learning, this study compares the performance of the proposed TIEO algorithm with three MPPT approaches: the recently developed metaheuristic algorithm known as the Football Training Team Algorithm (FTTA), the reinforcement learning-based Deep Q-Network (DQN), and the classical Perturb and Observe (P&O) method. As shown in Fig. 7, it can be seen that the P&O algorithm struggle to escape local optimum points, whereas the DQN, FTTA and the proposed TIEO approaches successfully converge to the global optimum point. However, both the DQN and FTTA require more time to reach the GMPP compared to TIEO.

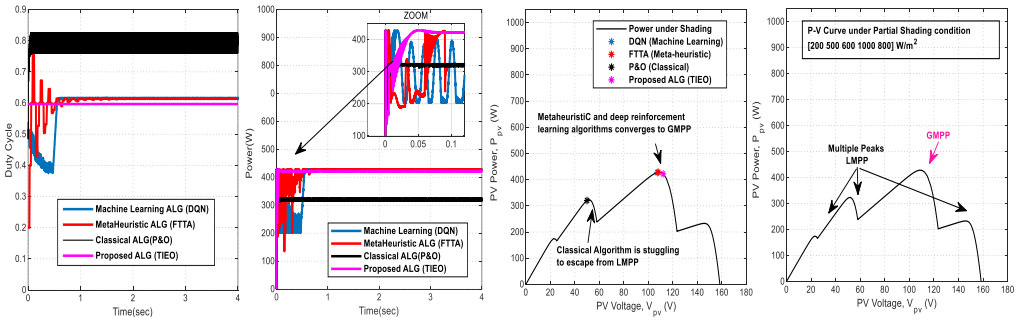

Fig. 7. Power and duty cycle responses of TIEO compared to DQN, FTTA and P&O

Expanding upon recent developments, the presented table (Table 1) extends the analysis by benchmarking the proposed algorithm (TIEO) against several MPPT techniques reported in the literature, as summarized in Table 2; the period during which each method was first applied to PV MPPT is also included. The comparison considers tracking efficiency, convergence time, and adaptability under DC and AC loads. Particle Swarm Optimization (PSO), the DQN, and TIEO perform well overall, but TIEO stands out with faster convergence and 98.6% tracking efficiency, demonstrating superior effectiveness and robustness.

Table 1. Summary comparison of existing MPPT algorithms and the proposed TIEO approach

MPPT-ALG	First applied to MPPT-PV	Tracking efficiency (%)	Convergence speed (sec)	Accuracy	Oscillations	Speed		
		Irradiation variation with DC load					PSC with load	
							DC	AC
CLASSICAL ALG [37]	P&O (1980)	100	0.022	High	Low	Fast	Poor	Poor
	INC (2000)	100	0.020	High	Low	Fast	Poor	Poor
	HC (1990)	98	0.015	Mod	Low	Fast	Poor	Poor
INTELLIGENT ALG [37]	FLC (1990)	99.4	0.010	High	Low	Fast	Mod	Mod
	ANN (1990)	99.7	0.005	High	Low	Fast	Mod	Poor
	ANFIS (2000)	99.6	0.010	High	Low	Low	Mod	Mod
	Machine Learning (2018–2023) **DQN**	**100**	**0.240**	**High**	**Low**	**Fast**	**High**	**High**
	Machine Learning (2018–2023) SVR	100	0.010	High	Low	Fast	Mod	Poor
	Machine Learning (2018–2023) SOM	95.2	0.015	Mod	Low	Fast	Mod	Mod
META-HEURISTIC ALG [37]	**PSO** (2000)	**100**	**Slow**	**High**	**Low**	**Mod**	**High**	**High**
	FPA (2015)	94.00	**Slow**	Mod	Low	Mod	High	High
	CSA (2013)	99.9	**Slow**	High	Low	Mod	High	High
	ABC (2012)	93	**Slow**	Mod	Low	Mod	High	High
	GA (1993)	95.5	**Slow**	Mod	Mod	Mod	High	Mod
	FTTA (2024)	99.8	0.75	High	Mod	Mod	High	Poor
PROPOSED ALG	**TIEO (2025)**	**98.6**	**0.05**	**High**	**Low**	**Fast**	**High**	**High**

HC: Hill Climbing, SVR: Support Vector Regression (supervised learning), SOM: Self-Organized Map (unsupervised learning), DQN (reinforcement learning), PSO: Particle Swarm Optimization, FPA: Flower Pollination Algorithm, CSA: Cuckoo Search Algorithm, ABC: Artificial Bee Colony, GA: Genetic Algorithm, Mod: Moderate, Slow: convergence speed (more than 0.75sec), PSC with Load: DC (resistance load), AC Load (pumping system)

Table 2. Overview of MPPT algorithms: features, learning and convergence

MPPT-algorithms		Learning mechanism	Algorithmic features	Convergence behavior	Advantages	Limitation
CLASSICAL ALG	**P&O (1980)**	Periodically perturbs duty cycle and observes ΔP	Fixed step-size iterative search	Moderate; oscillates near MPP	Simple, low-cost, easy to implement	Poor under PSC, It struggles to escape from LMPP
META-HEURISTIC ALG	**FTTA (2024)**	Simulates training, selection, and adaptation of football players	Team-based cooperative learning for GMPP optimization	Slow but stable	Strong balance between local and global search; avoids stagnation	Loss of population diversity, High computational cost
MACHINE LEARNING ALG	**DQN (2013)**	Reinforcement learning via Q-value neural estimation	Action-reward exploration for GMPP tracking	Slow but adaptive	Learns dynamically under shading	Requires training time and computational load
PROPOSED ALG	**TIEO (2025)**	Bio-inspired adaptive exploration–exploitation	Dynamic adaptation using autonomy, diplomacy, and war phases	Fast and stable	Excellent GMPP performance, self-learning	High computational cost

Figure 8 shows duty cycle and power response under extreme battery SOC conditions (5% and 99%) for the same weather variations in irradiance, temperature, and wind speed. In the low-SOC case, excess energy is sent to the dump load, while in the high-SOC case, it charges the battery.

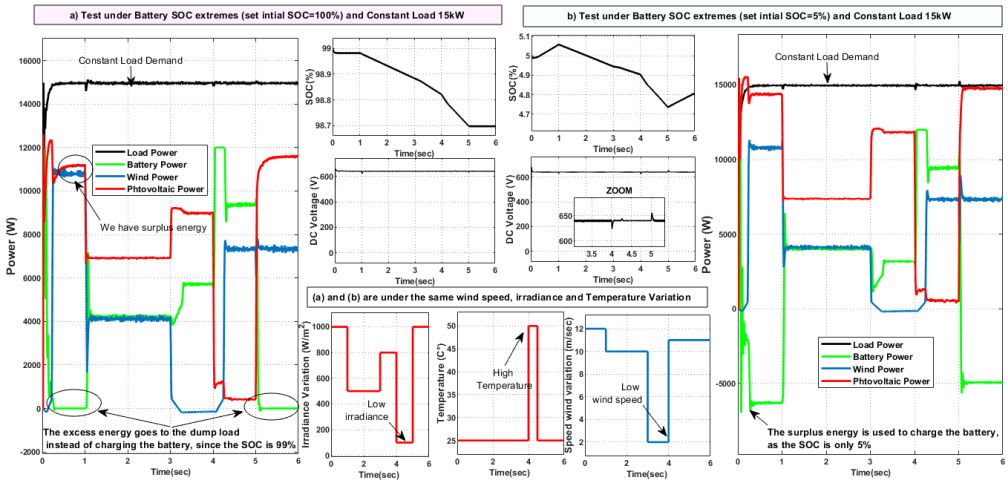

Fig. 8. Power and DC voltage response under weather variation and battery SOC extremes

Figures 9 and 11 show the transient response of the developed hybrid energy system under varying environmental conditions. The PV and wind boost converter duty cycles remain around 0.5 with minor fluctuations, indicating stable operation and efficient MPPT near each source's optimal power point.

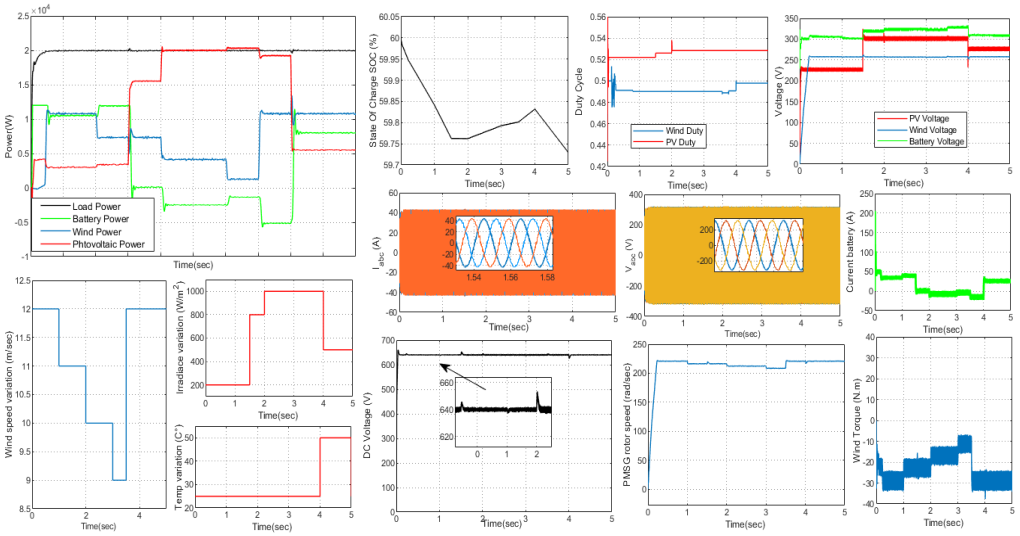

Fig. 9. Dynamic responses of the hybrid PV-Wind-Battery System under constant load demand (20 kW)

Figure 9 shows sinusoidal load voltage and current, with the DC bus voltage held at 640 V. The system remains stable under environmental disturbances, and the wind turbine torque varies linearly with wind speed, reflecting its aerodynamic behavior. Table 3 includes quantitative metrics like tracking efficiency (%), settling time and energy harvested (kW) across scenarios of Fig. 9.

Table 3. Performance metrics of TIEO algorithm under various operating conditions

Scenarios			**Settling time (sec)**				**Energy harvested (kW)**					**Effi-ciency (%)**
Time	**Weather variation**		**PV**	**Wind**	**Battery**	**Load**	**PV**	**Wind**	**Battery**	**Demand load**	**Dump load**	**Demand load**
0-1 (sec)	Wind speed 12 (m/sec)	Temp = 25° Irr = 200 W/m^2	0.05	0.2	0.02	0.2	3.1	10.9	10.8	20	4.8	99.9
1-1.5 (sec)	Wind speed = 11 (m/sec)	Temp = 25° Irr = 200 W/m^2	0.02	0.02	0.05	——	3.5	7.4	12		2.9	
1.5-2 (sec)	Wind speed = 11 (m/sec)	Temp = 25° Irr = 800 W/m^2	0.02	0.02	0.04	——	15.5	7.4	0		2.9	
2-3 (sec)	Wind speed = 10 (m/sec)	Temp = 25° Irr = 1000 W/m^2	0.02	0.02	0.04	——	20	4.1	–2.5		2.1	

Table continued on the next page

Table continued from the previous page

Scenarios			Settling time (sec)				Energy harvested (kW)					Effi-ciency (%)
Time	**Weather variation**		**PV**	**Wind**	**Battery**	**Load**	**PV**	**Wind**	**Battery**	**Demand load**	**Dump load**	**Demand load**
3-3.5 (sec)	Wind speed = 9 (m/sec)	Temp = 25° Irr = 1000 W/m^2	0.01	0.05	0.04	——	20.3	1.2	–1.4		0.1	
3.5-4 (sec)	Wind speed = 12 (m/sec)	Temp = 25° Irr = 1000 W/m^2	0.02	0.02	0.04	——	19.3	11	–5	20	5.3	99.9
4-5 (sec)	Wind speed = 12 (m/sec)	Temp = 50° Irr = 500 W/m^2	0.01	——	0.04	—-	5.5	10.7	8		4.2	

The irradiance profile begins at 200 W/m^2 (0–1.5 s), increases to 800 W/m^2 (1.5–2 s), peaks at 1000 W/m^2 (2–4 s), and finally drops to 500 W/m^2 (4–5 s). The ambient temperature is maintained constant at 25°C until 4 s, after which it rises to 50°C. Concurrently, wind speed varies as follows: 12 m/s (0–1 s), 11 m/s (1–2 s), 10 m/s (2–3 s), 9 m/sec (3–3.5 s), and returns to 12 m/sec between 3.5–5 s. These variations directly affect the power that is accessible from wind and photovoltaic sources. The Energy Sorage System (ESS) operates in discharge mode (from 0 to 2 s), as evidenced by the decreasing State of Charge (SOC). Between 2.5 and 4 s, the ESS transitions to charging mode as renewable generation exceeds the load demand. However, beyond 4 s, the reduction in irradiance combined with elevated temperature results in diminished PV output. Consequently, the ESS resumes discharging to bridge the energy deficit and ensure uninterrupted load supply.

Throughout the simulation period, power contributions from the PV array, wind turbine, and ESS dynamically adjust to maintain the constant 20 kW load. During the initial phase (0–1.5 s), the low irradiance (200 W/m^2) limits PV output to approximately 4 kW, while the wind turbine delivers up to 10 kW (notably during 0–1 s). In the second phase (2–4 s), under favorable irradiance and stable temperature, the PV output significantly increases, reaching around 20 kW, and becomes the primary source. Wind power output follows the wind speed trend, except during the 3.5–4 s interval, where it briefly reaches ~10 kW. The surplus energy in this phase leads to battery charging, as indicated by negative power or battery current values (as shown in the corresponding figure). In the final phase (4–5 s), the PV output drops to ~5 kW due to reduced irradiance and elevated temperature, while wind power stabilizes near 10 kW.

To maintain uninterrupted power delivery, the ESS resumes discharging. Finally, the DC bus voltage effectively tracks the reference voltage (640 V). The load voltage THD, Total Harmonic Distortion obtained (2.14%) is lower than the standard permissible limit of 5%, thereby validating the system's capability to kept high power quality during transient operating conditions (as illustrated in Fig. 10).

During the period from 0 to 2 s, the Energy Storage System (ESS) is discharging, with a noticeable decrease in the State of Charge (SOC). From 2.5 to 4 s, the ESS begins to charge as the renewable generation exceeds the load demand. However, after 4 s, due to the combined impact of reduced irradiance and elevated temperature (which decreases PV efficiency), the total generated power becomes insufficient. Consequently, the ESS resumes discharging to compensate for the energy deficit and ensure continuous load supply.

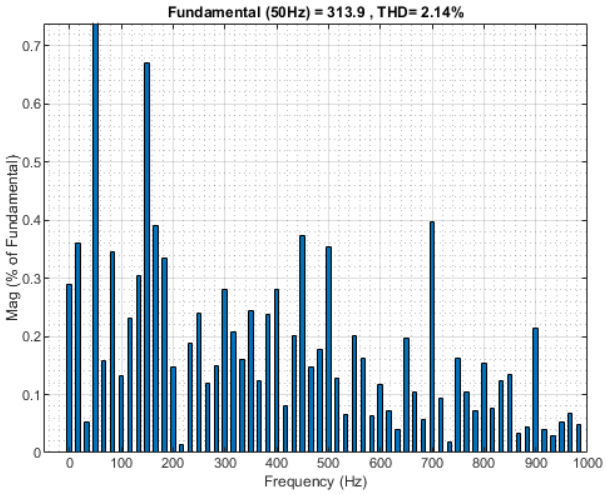

Fig. 10. Frequency spectrum of load voltage (FFT analysis)

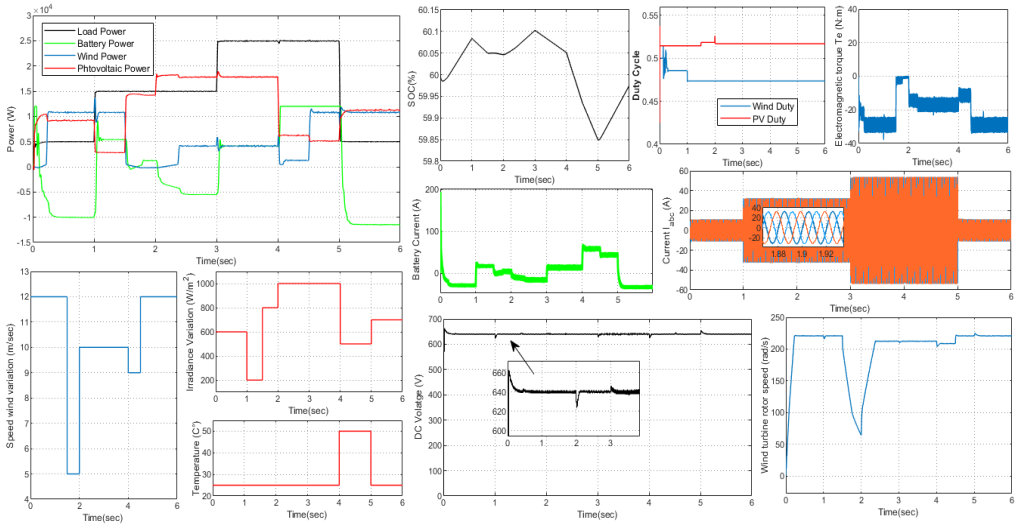

Fig. 11. Dynamic responses of the hybrid PV-Wind-Battery System under variable load demand (20 kW)

Throughout the simulation, the power contributions from PV, wind, and battery sources vary dynamically to maintain the constant 20 kW load. In the first phase (0–1.5 s), low irradiance (200 W/m^2) limits PV output to around 4 kW, while wind provides up to 10 kW (0–1 s). During the second phase (2–4 s), under optimal irradiance and stable temperature, PV output increases significantly and reaches around 20 kW, becoming the dominant source. The wind decreases proportional with wind speed decreasing except between 3.5–4 s, where it briefly supplies ~10 kW. During this period, excess energy causes the battery to charge (indicated by negative power or

negative battery current as shown figure). In the third phase (4–5 s), reduced irradiance and elevated temperature cause the PV output to drop to ~5 kW, while wind stabilizes near 10 kW. The battery resumes discharging to offset the deficit and guarantee uninterrupted load supply. the DC bus voltage response follows the desired voltage (640 V). The load voltage THD (2.12%) is lower than the standard value (5%).The previous scenario confirmed stable system operation under a constant 20 kW load, with regulated DC voltage (~640 V), duty cycles around 0.5, sinusoidal load current, and effective MPPT. In the current case, a variable load profile (5 kW → 15 kW → 25 kW → 5 kW) is employed to evaluate the system's dynamic performance. The DC bus voltage remains well-regulated at approximately 640 V throughout the load changes. Duty cycles of the PV and wind converters stay close to 0.5, and the PMSG continues to exhibit consistent torque and speed behavior. The Energy Storage System (ESS) responds adaptively, charging during times of excess generation and discharging during power shortfalls, based on real-time variations in irradiance, temperature, wind speed, and load demand. The load current waveform remains sinusoidal, with amplitude variations reflecting the changing load, demonstrating that the proposed hybrid system effectively maintains power quality and operational stability under variable conditions.

7. Hardware discussion

The proposed algorithm employs a 10×5 Q-table and 15 agents distributed across three tribes, resulting in a lightweight optimization framework. The computational complexity of the algorithm is approximately Q(15) per iteration, since each iteration updates 15 agents with simple arithmetic and Q-learning operations, making it efficient for real-time execution. The memory footprint is also minimal, requiring roughly 2–4 KB of RAM, primarily for storing the Q-table, agent attributes and persistent variables. Such low computational and memory demands make the algorithm highly suitable for real-time embedded implementation on both STM32 and ESP32 (for IoT-connected MPPT applications), where it can operate within tight timing and resource constraints.

8. Conclusion, limitation and future research directions

The TIEO-MPPT control strategy proposed in this study has been implemented for both PV and wind sources within a hybrid PV–Wind–Battery System. Unlike conventional methods, TIEO-MPPT intelligently adapts to environmental and load variations through its evolutionary learning mechanism. Simulation results confirm that the proposed approach ensures stable DC-bus voltage regulation (~640 V), maintains high power quality (low THD), and achieves a fast dynamic response under varying irradiance, temperature, wind speed, and load conditions. The Energy Storage System (ESS) effectively balances power flow and enhances system stability, while MPPT is achieved with minimal oscillations and high convergence accuracy.

Despite these promising results, certain limitations remain. Scalability and real-time computational constraints may arise as system size increases, leading to higher processing and memory demands on resource-constrained embedded platforms (e.g., ESP32, STM32). Moreover, the algorithm assumes ideal coordination, whereas practical stand-alone hybrid systems may experience delays, noise, and measurement inaccuracies that could affect MPPT efficiency and stability. Future

research should focus on Hardware-in-the-loop (HIL) validation to verify real-time performance under realistic converter behavior in stand-alone operation. Although this work considers a static load with varying demand, future studies should extend the analysis to other load types, such as dynamic, inductive, or motor-driven loads, to provide a more comprehensive evaluation of stand-alone system behavior. Additionally, incorporating adaptive SOC thresholds and self-tuning learning parameters will further enhance storage efficiency and overall system reliability.

In this work the major components used in the system as shown Fig. 1, are:

- MPPT-algorithm: TIEO is applied using Ntribe = 3, Nindividual = 5, $\alpha = 0.3$, $\gamma = 0.6$, $\beta = 0.4$, $\eta = 0.1$ (learning rate), $\varsigma = 0.9$ (discount factor), $\varepsilon = 0.1$ (exploration rate), Dmin = 0.05, Dmax = 0.95 (boundaries to avoid extremes), Q-table is initialized as zeros or small random numbers, Itermax = 5 000, 15 agents, Q-table dimension = 50 Q-values;
- PV source: 81 panel of 270 W connected 9 in series and 9 in parallel, total – 20 kW, V_{mp} – 30.8 V/panel, I_{mp} – 8.77 A, $N_{\text{cells}} = 60$, $V_{oc} = 37.9$ V, $I_{sc} = 9.07$ A, $R_{sh} = 2185.1547$ Ohm, $R_s = 0.26166$ Ohm;
- Wind source: PMSG is a 12 kW-class Permanent Synchronous Magnet Synchronous Generator, operating at torque – 67.27 N·m, speed – 1700 rpm, DC voltage output – 560 V and the nominal mechanical output power turbine is 10 kW;
- PMSG: pre-set model – 14–76.27 Nm, 560 V_{dc}, 1700 rpm–70.2 N·m;
- Battery: Ni-MH, 60.5 Ah capacity, initial SOC – 60% and 300 V nominal voltage;
- Inverter: 3-phase 2-level VSI, DC input – 640 V, switching frequency – 20 kHz;
- PV DC-DC converter: unidirectional boost converter, input voltage rate – 280–350 V, switching frequency – 20 kHz;
- Battery DC-DC converter: bidirectional buck-boost converter, input voltage rate – 250–350 V, switching frequency – 20 kHz;
- Wind energy converter: AC–DC rectifier + boost converter, input voltage rate – rectified DC 480 – 560 V, switching frequency – 20 kHz;
- Grid: three phase static load (first scenario: 20 kW, second scenario: variable load values);
- Simulation settings: sampling time: $10e^{-6}$ s, solver type – ode23t (mod.stiff/trapezaoidal).

References

[1] Yang B., Jian L., Wang L., Yao W., Wu Q.H., *Nonlinear maximum power point tracking control and modal analysis of DFIG based wind turbine*, International Journal of Electrical Power and Energy Systems, vol. 74, pp. 429–436 (2016), DOI: 10.1016/j.ijepes.2015.07.036.

[2] Karakasis N.E., Madamlis C., *High efficiency control strategy in a wind energy conversion system with doubly fed induction generator*, Renewable Energy, vol. 125, pp. 974–984 (2018), DOI: 10.1016/j.renene.2018.03.020.

[3] Fantino R., Solsona J., Busada C., *Nonlinear observer-based control for PMSG wind turbine*, Energy, vol. 113, pp. 248–257 (2016), DOI: 10.1016/j.energy.2016.07.039.

[4] Errami Y., Ouassaid M., Maaroufi M., *Performance comparison of a linear control for grid connected PMSG wind energy conversion system*, International Journal of Electrical Power and Energy Systems, vol. 68, pp. 180–194 (2015), DOI: 10.1016/j.ijepes.2014.12.027.

[5] Chen J., Yao W., Zang C.K., Ren Y., Jian L., *Design of robust MPPT controller for grid-connected PMSG-Based wind turbine via perturbation observation based nonlinear adaptive control*, Renewable Energy, Elsevier, vol. 134, pp. 478–495 (2019), DOI: 10.1016/j.renene.2018.11.048.

[6] Mohamed S.A., Abd El Sattar M., *A comparative study of P&O and INC maximum power point tracking techniques for grid-connected PV systems*, SN Applied Sciences, vol. 1, no. 174, pp. 1–13 (2019), DOI: 10.1007/s42452-018-0134-4.

[7] Baimel D., Tapuchi S., Levron Y., Belikov J., *Improved Fractional Open Circuit Voltage MPPT Methods for PV Systems*, Electronics, vol. 8, no. 3, pp. 321–341 (2019), DOI: 10.3390/electronics8030321.

[8] Ahmed J., Salam Z., *An improved perturb and observe (P&O) maximum power point tracking (MPPT) algorithm for higher efficiency*, Applied Energy, vol. 150, pp. 97–108 (2015), DOI: 10.1016/j.apenergy.2015.04.006.

[9] Subudhi B., Pradhan R., *A comparative study on maximum power point tracking techniques for photovoltaic power systems*, IEEE Transactions on Sustainable Energy, vol. 4, no. 1, pp. 89–98 (2013), DOI: 10.1109/TSTE.2012.2202294.

[10] Bollipo R.B., Mikkili S., Bonthagorla P.K., *Hybrid, optimization, intelligent and classical PV MPPT techniques: A Review*, CSEE Journal of Power and Energy Systems, vol. 7, no. 1, pp. 9–33 (2021), DOI: 10.17775/CSEEJPES.2019.02720.

[11] Cheikh M.A., Larbes C., Kebir G.T., Zerguerras A., *Maximum power point tracking using a fuzzy logic control scheme*, Revue des énergies Renouvelables, vol. 10, no. 3, pp. 387–395 (2007), DOI: 10.54966/jreen.v10i3.771.

[12] Lin W.M., Hong C.M., Chen C.H., *Neural-Network-Based MPPT Control of a Stand-Alone Hybrid Power Generation System*, IEEE Transactions on Power Electronics, vol. 26, no. 12, pp. 3571–3581 (2011), DOI: 10.1109/TPEL.2011.2161775.

[13] Femia N., Granozio D., Petrone G., Spagnuolo G., Vitelli M., *Predictive & adaptive MPPT perturb and observe method*, IEEE Transactions on Aerospace and Electronic Systems, vol. 43, no. 3, pp. 934–950 (2007), DOI: 10.1109/TAES.2007.4383584.

[14] Salman D., Khalif Elmi Y., Mohamed Isak A., Sheikh-Muse A., *Evaluation of MPPT Algorithms for Solar PV Systems with Machine Learning and Metaheuristic Techniques*, Mathematical Modelling of Engineering Problems, vol. 12, no. 1, pp. 115–124 (2025), DOI: 10.18280/mmep.120113.

[15] Katche M.L., Makokha A.B., Zachary S.O., Adaramola M.S., *A Comprehensive Review of Maximum Power Point Tracking (MPPT) Techniques Used in Solar PV Systems*, Energies, vol. 16, no. 5, pp. 2206–2229 (2023), DOI: 10.3390/en16052206.

[16] Abidi H., Sidhom L., Chihi I., *Systematic Literature Review and Benchmarking for Photovoltaic MPPT Techniques*, Energies, vol. 16, no. 8, pp. 3509–3554 (2023), DOI: 10.3390/en16083509.

[17] Boubaker O., *MPPT techniques for photovoltaic systems: a systematic review in current trends and recent advances in artificial intelligence*, Discover Energy, vol. 3, no. 9 (2023), DOI: 10.1007/s43937-023-00024-2.

[18] Worku M.Y., Hassan M.A., Maraaba L.S., Shafiullah M., Elkadeem M.R., Hossain M.I., Abido M.A., *A Comprehensive Review of Recent Maximum Power Point Tracking Techniques for Photovoltaic Systems under Partial Shading*, Sustainability, vol. 15, no. 14, pp. 11132–11160 (2023), DOI: 10.3390/su151411132.

[19] Endiz M.S., Gökku G., Cosgun A.E., Demir H., *A Review of Traditional and Advanced MPPT Approaches for PV Systems Under Uniformly Insolation and Partially Shaded Conditions*, Applied Sciences, vol. 15, no. 3, pp. 1031–1063 (2025), DOI: 10.3390/app15031031.

[20] Douifi N., Abbadi A., Hamidia F., Yahya K., Mohamed M., Rai N., *A Novel MPPT Based Reptile Search Algorithm for Photovoltaic System under Various Conditions*, Applied Sciences, vol. 13, no. 8, pp. 48664–48678 (2023), DOI: 10.3390/app13084866.

[21] Mhanni Y., Lagmich Y., *Adaptive metaheuristic strategies for optimal power point tracking in photovoltaic systems under fluctuating shading conditions*, EPJ Photovoltaics, vol. 15, no. 31, pp. 1–16 (2024), DOI: 10.1051/epjpv/2024026.

[22] Rashmi G., Linda M.M., *A novel MPPT design for a wind energy conversion system using grey wolf optimization*, Automatika, vol. 64, no. 4, pp. 798–806 (2023), DOI: 10.1080/00051144.2023.2218168.

[23] Hassanien R., Abdel-Raheem Y., Hossam H.H.M., Essam E.M.M., *An efficient variable-step P&O maximum power point tracking technique for grid-connected wind energy conversion system*, SN Applied Sciences, vol. 1, no. 1658, pp. 1–14 (2019), DOI: 10.1007/s42452-019-1716-5.

[24] Sierra-García J.E., Santos M., *Neural networks and reinforcement learning in wind turbine control*. Revista Iberoamericana de Automatica e Informatica Industrial, vol. 18, pp. 327–335 (2021), DOI: 10.4995/riai.2021.16111.

[25] Vu N.T.T., Nguyen H.D., Nguyen A.T., *Reinforcement Learning-Based Adaptive Optimal Fuzzy MPPT Control for Variable Speed Wind Turbine*, IEEE Access, vol. 10, pp. 95771–95780 (2022), DOI: 10.1109/ACCESS.2022.3205124.

[26] Chen J., Yao W., Zhang C.-Ke., Rend Y., Jiang L., *Design of robust MPPT controller for grid-connected PMSG-based wind turbine via perturbation observation based nonlinear adaptive control*, Renewable Energy, vol. 134, pp. 478–495 (2019), DOI: 10.1016/j.renene.2018.11.048.

[27] Yang B., Yu T., Shu H., Han Y., Cao P., Jiang L., *Adaptive fractional-order PID control of PMSG-based wind energy conversion system for MPPT using linear observers*, International Transactions Electrical Energy Systems, vol. 29, no. 1, pp. 2–18 (2019), DOI: 10.1002/etep.2697.

[28] Rabah S., Zaier A., Lloret J., Dahman H., *Efficiency Enhancement of a Hybrid Sustainable Energy Harvesting System Using HHHOPSO-MPPT for IoT Devices*, Sustainability, vol. 15, no. 13, pp. 10252–10280 (2023), DOI: 10.3390/su151310252.

[29] Giraldo L.F., Gaviria J.F., Torres M.I., Alonso C., Bressan M., *Deep reinforcement learning using deep-Q-network for Global Maximum Power Point tracking: Design and experiments in real photovoltaic systems*, Heliyon, vol. 10, e37974 (2024), DOI: 10.1016/j.heliyon.2024.e37974.

[30] Yılmaz M., Çorapsız M.F., *A robust MPPT method based on optimizable Gaussian process regression and high order sliding mode control for solar systems under partial shading conditions*, Renewable Energy (2025), DOI: 10.1016/j.renene.2025.122339.

[31] Koshkarbay N. *et al.*, *Improved MPPT technology for PV systems using Social Spider optimization (SSO): Efficient handling of partial shading and load variations*, Electric Power Syst. Res. (2025).

[32] Sharma S., Chauhan B., Kumar Saxena N., *Artificial Neural Network Grid-Connected MPPT-Based Techniques for Hybrid PV-WIND with Battery Energy Storage System*, Journal of the Institution of Engineers (India) Series B (2023), DOI: 10.1007/s40031-023-00922-y.

[33] Mauludin M.S., Khairudin M., Asnawi R., *Optimization of a Hybrid PV-Wind Power System for Enhancing Efficiency and Power Quality Using MATLAB/SIMULINK Simulations*, Journal Européen des Systèmes Automatisés, vol. 58, no. 4, pp. 823–832 (2025), DOI: 10.18280/jesa.580416.

[34] Osama L., Salah A., Saleh S.M., Kourany M., *Meta-heuristic Optimization for Wind Turbine Control: Evaluating Performance with PI and Fractional PI Controllers for Maximum Power Extraction*, Journal of Electrical Systems, vol. 20, no. 3, pp. 7968–7982 (2024), https://journal.esrgroups.org/jes/article/view/7795.

[35] Yao Ye, Hong Xiaoxi, Lei Xiong, *Study on a new metaheuristic algorithm -Tribal intelligent evolution optimization and its application in optimal control of cooling plants*, Applied Energy, Elsevier, vol. 383 (2025), DOI: 10.1016/j.apenergy.2025.125339.

[36] Hong X., Yao Y., Wang K., Yang J., Liu W., *Energy-saving Optimal Control of Secondary District Cooling System Based on Tribal Intelligent Evolution Optimization Algorithm*, Energy, vol. 316, no. 1 (2025), DOI: 10.1016/j.energy.2025.134554.

[37] Hamidia F., Abbadi Amel, Medjber A., Salhi F., Hamil A., Skender M.R., *Enhanced MPPT Algorithms for PV panels: Review and Comparative Study*, International Conference ICAIRES (2025), https://icaires.com/.